The following scientific article was officially published in the journal *Medical Engineering & Physics*, published by Elsevier. This article's citation is as follows:

Grenier, Sébastien, Stefan Parent, and Farida Cheriet. "Personalized 3D reconstruction of the rib cage for clinical assessment of trunk deformities." Medical Engineering & Physics, Vol. 35, no. 11 (2013): pp. 1651-1658.

doi: 10.1016/j.medengphy.2013.06.002

The manuscript, in its revised form prior to final acceptance by the publisher, is reproduced in the following pages.

IPEM, 2013

© 2013 Institute of Physics and Engineering in Medicine. This work is licensed under the Creative Commons Attribution-NonCommercial-NoDerivatives 4.0 International License. To view a copy of this license, visit:
http://creativecommons.org/licenses/by-nc-nd/4.0/

Elsevier Editorial System(tm) for Medical Engineering & Physics
Manuscript Draft

Manuscript Number: MEP-D-12-00464R2

Title: Personalized 3D reconstruction of the rib cage for clinical assessment of trunk deformities

Article Type: Paper

Section/Category: Regular Issue Paper

Keywords: 3D reconstruction; Predictive model; Semi-automatic segmentation; Rib cage; X-rays; Clinical assessment; Scoliosis

Corresponding Author: Mr. Sebastien Grenier, M.Sc.A

Corresponding Author's Institution: École Polytechnique de Montréal

First Author: Sebastien Grenier, M.Sc.A

Order of Authors: Sebastien Grenier, M.Sc.A; Stefan Parent, MD; Farida Cheriet, Ph.D

Abstract: Scoliosis is a 3D deformity of the spine and rib cage. Extensive validation of 3D reconstruction methods of the spine from biplanar radiography has already been published. In this article, we propose a novel method to reconstruct the rib cage, using the same biplanar views as for the 3D reconstruction of the spine, to allow clinical assessment of whole trunk deformities. This technique uses a semi-automatic segmentation of the ribs in the postero-anterior X-ray view and an interactive segmentation of partial rib edges in the lateral view. The rib midlines are automatically extracted in 2D and reconstructed in 3D using the epipolar geometry. For the ribs not visible in the lateral view, the method predicts their 3D shape. The accuracy of the proposed method has been assessed using data obtained from a synthetic bone model as a gold standard and has also been evaluated using data of real patients with scoliotic deformities. Results show that the reconstructed ribs enable a reliable evaluation of the rib axial rotation, which will allow a 3D clinical assessment of the spine and rib cage deformities.

Manuscript
Click here to view linked References

Personalized 3D reconstruction of the rib cage for clinical assessment of trunk deformities

Sébastien Grenier[-* 1,2], M.Sc.A, Stefan Parent[2], M.D., Farida Cheriet[1,2], Ph.D

[1] École Polytechnique de Montréal, Montreal, Canada

[2] Sainte-Justine Hospital Research Center, Montreal, Canada

* Corresponding author: sebastien-3.grenier@polymtl.ca

Abstract

Scoliosis is a 3D deformity of the spine and rib cage. Extensive validation of 3D reconstruction methods of the spine from biplanar radiography has already been published. In this article, we propose a novel method to reconstruct the rib cage, using the same biplanar views as for the 3D reconstruction of the spine, to allow clinical assessment of whole trunk deformities. This technique uses a semi-automatic segmentation of the ribs in the postero-anterior X-ray view and an interactive segmentation of partial rib edges in the lateral view. The rib midlines are automatically extracted in 2D and reconstructed in 3D using the epipolar geometry. For the ribs not visible in the lateral view, the method predicts their 3D shape. The accuracy of the proposed method has been assessed using data obtained from a synthetic bone model as a gold standard and has also been evaluated using data of real patients with scoliotic deformities. Results show that the reconstructed ribs enable a reliable evaluation of the rib axial rotation, which will allow a 3D clinical assessment of the spine and rib cage deformities.

Keywords

3D reconstruction; Predictive model; Semi-automatic segmentation; Rib cage; X-rays; Clinical assessment; Scoliosis.

1. Introduction

Adolescent idiopathic scoliosis (AIS) is a three-dimensional deformity of the spine and rib cage. To diagnose the severity of the scoliosis, an evaluation is done by measuring the Cobb angles on frontal and lateral radiographs. However, it has been shown that AIS is more complex than a biplanar deformation [1, 2], and as such a 3D evaluation is important. Over the past years, several studies have focused on the deformity of the spine. Many reliable clinical assessments and classifications for the spine have been proposed [3-6]. However, AIS also implies a deformation of the rib cage [7, 8] and current 3D

reconstruction techniques for the rib cage still do not provide a reliable 3D clinical assessment of the rib cage deformities.

These reconstruction techniques can be classified into two categories : those that reconstruct the rib cage using two radiographic views in the frontal plane, i.e. the postero-anterior (PA-0) view and postero-anterior view with the X-ray tube angled at 20° (PA-20), which we will refer to as the PA-20 reconstruction methods (PA20-RM), and those that reconstruct the rib cage using the standard radiographic views, i.e. the PA-0 and lateral (LAT) views, which we will refer to as the LAT reconstruction methods (LAT-RM).

Dansereau *et al.* [9] first reported a method to reconstruct the rib cage using two radiographs in the postero-anterior plane : PA-0 and PA-20. The method requires a manual selection of 11 points for each rib midline on the two X-rays. A cubic spline is then fitted along these points and a discretization into 60 points is done for all ribs. The discretized points from both radiographs are then matched and reconstructed in 3D using the Direct Linear Transform (DLT) algorithm. The entire rib cage can be easily reconstructed in 3D since there is good visibility of the ribs in both views (PA-0 and PA-20) compared to the lateral view (LAT). However, the manual selection of rib midline points leads to errors because of the difficulty in selecting the pixels representing the true midline and in their matching between the pair of views. The method was upgraded to take into account the displacement of the patient's rib cage between the two acquisitions [10], but the precision of the 3D reconstruction is still lacking.

In order to limit the patients' exposure to X-ray radiation, researchers have developed new techniques to reconstruct the rib cage from only the PA-0 and LAT views, which are the standard clinical radiographic views used for the reconstruction of the spine. Some of these techniques [11-13] propose new methods to accelerate the process of reconstructing each rib by requiring fewer manual selections, making them more robust to human error. Séoud *et al.* [13] uses the two standard X-rays and requires only five points per rib. The five points are reconstructed in 3D, and a paraboloid is fitted on these points. Then M additional

points are interpolated on this paraboloid. Finally, a cubic spline is fitted to all these points and represents the final rib. This work showed that by using the standard views (PA-0 and LAT), the reconstruction gives better results than [9] and therefore is a better approach for the patient because it implies less radiation. However, due to visibility constraints, only the lower section of the rib cage can be reconstructed, i.e. the ribs that are clearly distinguishable in the two radiographs.

Others have proposed techniques to reconstruct the rib cage in 3D using silhouettes and average rib cages. Benameur *et al.* [11] used a statistical method to reconstruct the entire rib cage. To reconstruct a given rib cage, an average rib cage is generated and deformed until its projections in the PA-0 and LAT match the rib cage identified on the radiographs. In [14], the shape of a rib to reconstruct is extracted in each radiograph. Different training shapes are then deformed using a statistical shape model (SSM) to obtain a specific model for the patient. These models are deformed so that their projections match the silhouettes extracted in each radiograph. More recently, Koehler and Wischgoll [15] proposed a new technique that uses the semi-automatic rib detection algorithm proposed by Plourde *et al.* [16]. First, the ribs are detected in the frontal radiograph, and the rib cage boundary is segmented interactively in the lateral view. Then, a primitive template (or half-torus), similar to a real rib, is generated. One problem is that their reconstruction does not respect the true form of a rib because they use a half-torus with an arbitrary circular cross section. Furthermore, the projection used is orthogonal, which is a simplification of the radiographic projection. We also note that none of these techniques have undergone extensive quantitative evaluation of their precision. Thus, there is not enough evidence supporting their clinical use for 3D clinical assessment of rib cage deformities.

Thus, the goal of the present study is to provide and validate a new technique to reconstruct the rib cage with adequate accuracy for a clinical assessment of human trunk deformities. We propose a novel method based on a semi-automatic segmentation followed by a reconstruction of the visible ribs and an intra-patient prediction of the occluded ribs. This method is applicable to any system that uses biplanar projection, including the EOS low dose radiographic system [17].

2. Materials and Methods

2.1. Data Acquisition

To validate the proposed method, a cohort of 15 patients with moderate or severe AIS from Sainte-Justine Hospital (SJH) in Montreal, Canada was used for this study. The average age and Cobb angle of 10 patients were 12.6 years (±1 year) and 33.5° (±7°) respectively, while the mean age and Cobb angle of the remaining 5 patients were respectively 15.4 years (±1.1 years) and 51.6° (±7.1°).

The proposed method uses the standard postero-anterior (PA-0) and lateral (LAT) radiographs of the whole trunk routinely acquired in upright position in the frontal and lateral planes at SJH. The images were acquired using a Fuji FCR7501S X-ray imaging system. A rotary platform was used to bring the patient from the LAT to the PA-0 position. In order to prevent involuntary movement due to posture and position change, the platform included a stabilization device composed of elbow supports and handlebars [18]. These were adjusted so that the lower arms were horizontal and aimed frontward while the upper arms were angled backward at approximately 45°. To calibrate the system, the patient wore a jacket composed of sixteen embedded radio-opaque markers and a non linear optimization procedure [19] was performed to determine the parameters of each radiographic projection. In addition, trunk surface topography was acquired for the 10 patients with moderate AIS on the same visit dates in standing posture using an optical digitizing system at the SJH orthopedic clinic [20].

2.2. 3D Reconstruction of the Spine and the Lower Rib Cage

Six anatomical landmarks per vertebra are then manually selected in both views and reconstructed in 3D [21]. The spine is thus entirely reconstructed in 3D. The coordinate system of the reconstructed spine and rib cage is as follows: X axis points toward the front of the patient, Y axis points toward the left and Z axis points upward. Furthermore, the 3D reconstructed landmarks are used to adjust a generic vertebral model in order to complete the geometry [22]. These landmarks are then used to determine the insertion points of the ribs, which are the head and the tubercle of the rib. According to rib cage anatomy [23, 24], the ribs of levels T1 to T10 are articulated with the vertebrae of the same levels at these two points. The

head of the i^{th} rib lies between the superior articular facet (SAF) of the i^{th} thoracic vertebra and the inferior articular facet (IAF) of the body of the $(i-1)^{th}$ thoracic vertebra. The tubercle of the i^{th} rib is joined to the articular facet of the transverse process (AFTP) of the thoracic vertebra of the same level. The midpoint of the head (H) and tubercle (T) are computed using the following formulae:

$$H_{i,j} = \left(IAF_{i-1,j} + SAF_{i,j}\right)/2 \quad (1)$$

$$T_{i,j} = c_{i,j} + d.\vec{n}_{i,j} \quad (2)$$

where i and j are respectively the thoracic level (1 to 10) and the side (1 for left, 2 for right); $c_{i,j}$ is the centroid of the N landmarks forming the AFTP, $\vec{n}$ is the normal vector of the least squares plane of the N landmarks and d is the average distance between c and T, which is fixed at 7.09 mm [13, 25]. Fig. 1 shows the location of the rib attachment points on the adjacent vertebrae. The floating ribs T11 and T12 are only connected to the spine by their heads which are directly attached to the SAFs of the same levels. This is the same technique used by [13] to generate the insertion points of the ribs.

To reconstruct the lower part of the rib cage, the ribs have to be detected in both views. To do so, we use the algorithm developed by Plourde *et al.* [16]. This allows us to extract the ribs' edges in the PA-0, not just their midlines, by manually inputting only four points per rib. Fig. 2a shows a typical detection of a rib in the PA-0 view. In the lateral view, we detect the contours of each rib from a set of interactively selected edge points. A spline is then fitted on those points and represents the rib's edges. It is imperative that the most posterior point and the most anterior one be selected. Fig. 2b shows a rib segmentation in the LAT view.

For each detected rib, the midline is computed in each view. Then, we match every point between the most posterior and most anterior limits using epipolar geometry. This is achieved by finding the point in

the PA-0 view that is closest to the epipolar line corresponding to each point in the LAT view. Each 3D point associated with a pair of 2D points is then reconstructed by the triangulation method.

Having the reconstructed 3D points for a given rib, a paraboloid is fitted on these points using the same approach as Séoud *et al.* [13]. M points are then sampled along the paraboloid following the projection rays from the most posterior point to the most anterior one. Since we have the reconstruction of the head, tubercle and the M discretized points, it is possible to generate a cubic spline approximation of the complete rib midline.

2.3. 3D Reconstruction of the Upper Rib Cage

The previous procedure is generally applicable only for the lower portion of the rib cage, typically from levels T6 to T12. Due to the superposition of other structures, especially the arms, the visibility of the upper rib cage is seriously hampered in the lateral view [13]. In order to reconstruct the remaining undetected ribs, the first step is to generate a predictive model. This model results from a statistical analysis of a database of patients with previously 3D reconstructed rib cages. Our database is comprised of 40 real patients from SJH. 13 of these patients had moderate AIS and underwent subsequent brace treatment. Among these, the average Cobb angle and the mean age recorded at the time of consultation were respectively 36° (±8°) and 12.7 years (±1 year). The 27 other cases had severe AIS and underwent subsequent surgical treatment. The average Cobb angle and the mean age at the time of consultation for this subgroup were 60.3° (±12.4°) and 14.9 years (±1.4 years) respectively. All 40 patients had three X-ray acquisitions (PA-0, PA-20 and LAT), and their rib cages were reconstructed by the same operator with the technique described in [9].

Using this data, it is possible to learn the mean and standard deviation of the rib plane orientation for each vertebral level. A least squares plane is fitted on both ribs of a given level and the normal to that plane is projected onto the XZ plane. Doing this, the orientation becomes independent of the vertebra's axial and frontal rotations. Using spherical coordinates, we get a single value, φ, for each thoracic level. We then compute the mean and standard deviation of φ over the set of patients. Fig. 3 shows summary statistics

for the rib plane orientations for the 40 patients. These statistics are computed on the brace group, on the preoperative group, and all together. Fig. 3 illustrates that, except at the T12 level, the ribs lie in less vertical planes for the patients with moderate AIS than for the patients with severe AIS.

To estimate the shape of a rib, the reconstruction of the rib directly below it must be available. This means that the reconstruction of the rib cage is performed from bottom to top. The previous rib is translated to the position of the current one, from rib head to rib head. Since the ribs are not of the same size, we have to scale them. The compression (or extension) ratio is computed from the area of the current rib midline divided by the previous rib midline's area in the frontal radiograph:

$$Ratio_i = MidlineArea_i / MidlineArea_{i-1} \quad (3)$$

The rib midline area is defined as the region enclosed by the midline's spline curve and by the line joining the midline extremities (Fig. 4). Eq. (3) is used to compress the rib around its head in the lateral view. This is done by applying the scale factor along the X axis to the distance between each point and the head. This new distance modifies only the X coordinate of the point, making it closer or further away from the head. Then, using the $\tilde{\varphi}$ values computed from the database, we perform an optimization in order to find the value of φ in the range $\tilde{\varphi} \pm \sigma_{\varphi}$which yields the minimal projection error in the PA-0 view. At each iteration, the new φ value is used to rotate the rib around the Y-axis (centered on the rib head) and its 2D projection is then computed. This gives us an optimal rib plane orientation. The optimally placed new rib is used to generate a paraboloid, as with the lower rib cage levels, and M points are discretized along it following the projection rays from the most posterior point to the most anterior one.

2.4. Generation of the Contour Surface

In order to obtain a personalized rib geometry, instead of building a cylinder around the midline as in [15], we generate a ribbon-like open 3D surface that represent the rib's variable thickness. To generate this surface, we use the projection rays of the outer and inner contours of the rib in the PA-0 view. The outer and inner rays form two separate surfaces by triangulating the source point with the successive pairs of contour points. N points are sampled on the rib midline, and for each of them the nearest point is computed on the two surfaces. If any of the sampled points lie outside the detected contours, the minimal distances are extrapolated. This gives us three vertices, O, $M$and I, for each sampled point. To form the surface, we build four triangles between the set $\{O_i, M_i, I_i\}$ and $\{O_{i+1}, M_{i+1}, I_{i+1}\}$, for $i = 1..N-1$ (Fig. 5). The four triangles are:

$$T_1 = \{O_i, O_{i+1}, M_{i+1}\}$$

$$T_2 = \{O_i, M_{i+1}, M_i\}$$

$$T_3 = \{M_i, M_{i+1}, I_{i+1}\}$$

$$T_4 = \{M_i, I_{i+1}, I_i\}$$

2.5. Validation Method

First, the accuracy of the proposed method is assessed by comparing our results against a gold standard, i.e. a synthetic bone model representing the rib cage mounted on a radio-transparent frame (acrylic plastic), built with four vertical rods and two horizontal supports at the top and bottom. The model is attached to the frame with vinyl adhesive tape. Its dimensions are those of a young child. The maximal length of the spine is 56 cm. The maximal depth and width of the thoracic cage are 15 cm and 25 cm, respectively. The results obtained by Dansereau *et al.* [9], are also compared against the gold standard. Secondly, the robustness of our method is evaluated by comparing our results to those obtained by Séoud *et al.* [13]. Finally, our method is compared against Dansereau *et al.* [9] for clinical assessment. For all three validations, we use point to point distances. Furthermore, for the second validation (comparison

against Séoud *et al.* [13]), we also use clinical indices to find the correlation between the rib humps and the back surface rotation (BSR). All tests are conducted on an Intel Core i7 930 with 6 GB of RAM.

3. Results

Fig. 6 shows the reconstruction of a typical patient's rib cage. We can see the surface generated by our method, with the upper and lower contour, which represents exactly the ribs' variable thicknesses seen in the PA-0 view. The average reconstruction time is 20 seconds, with an average segmentation time of 40 minutes for both views, depending on the visibility of the ribs.

3.1. Gold Standard

For our gold standard, a synthetic model of a scoliotic spine and rib cage is digitized with the MicroScribe system [26]. The precision of the digitizer is 0.2 mm. Three configurations are considered: no deformity, a minor deformity with 20° of Cobb angle and a major deformity with 40° of Cobb angle. For each case, three radiographs (PA-0, PA-20 and LAT) are taken and the spine is first reconstructed. To evaluate the accuracy of the proposed method and the PA20-RM, the reconstructed rib cage is first registered with the ground truth by aligning the center of gravity of both models. Then point to point distances are computed between the reconstructed and digitized ribs. The mean distance d between the reconstructed and digitized points, in millimeters, determines the overall accuracy of the reconstruction.

Fig. 7 shows the results of our proposed method and of the PA20-RM against the digitized gold standard model. The mean distances for the proposed method are 11.95 mm (±6.56 mm), 9.30 mm (±5.86 mm) and 8.27 mm (±5.16 mm) for the 0°, 20° and 40° configurations, respectively. The mean distances for the PA20-RM are 23.98 mm (±11.09 mm), 11.80 mm (±6.56 mm) and 14.05 mm (±9.59 mm) for the 0°, 20° and 40° configurations, respectively. We can see that overall, the ribs reconstructed with the proposed method are closer at all thoracic levels to the ground truth than the ribs reconstructed with the PA20-RM. Ribs of level T10 for the 20° and 40° configurations are removed from the analysis because they are not visible on the radiographs. Note that no ribs need to be predicted because all the upper ribs are visible.

Furthermore, a synthetic model cannot represent the same characteristics as a statistical model obtained with real patients. Therefore, we choose not to use the prediction model in this case.

3.2. Comparison with the LAT-RM

In order to test whether our modification to the LAT-RM algorithm in [13] constitutes an improvement, the correlations between the rib axial rotations (RAR) obtained from both techniques and the back surface rotation (BSR) are compared. This provides a quantitative measure of the effects of using a semi-automatic rib edge detection instead of a manual selection. To compute the RAR for each rib pair, the ribs are projected on a horizontal plane and the angle formed by the dual-tangent to the projected rib pair's most posterior points and by the axis passing through the projected anterior superior iliac spines (hereafter called the horizontal ASIS line), expressed in degrees, forms the RAR. To compute the BSR, we use the trunk surface acquisitions. After an elastic registration of the trunk surface with the underlying bone structures, trunk cross-sections are extracted by computing the intersections of a set of horizontal planes, which are situated at the centroids of the thoracic vertebrae, with the trunk surface. Finally, the BSR is defined as the angle formed by the dual-tangent to the posterior side of each cross-section of the trunk surface and the horizontal ASIS line, expressed in degrees. This evaluation is done on the 10 brace patients used for validation in [13].

Table 1 shows a comparison between the number of reconstructed ribs for the proposed method and for the LAT-RM. All the ribs from levels T1 to T9 are reconstructed in our case, and only a few are missing for levels T10, T11 and T12. In such cases, the lower ribs are not distinguishable in the LAT radiograph, so they are not detected. Meanwhile, LAT-RM does not detect the upper cage in any of the cases. However, the comparison of the correlations between the RAR and the BSR can be done only for the ribs that are detected with both methods. The proposed method has a Pearson coefficient of 0.55 compared to 0.49 for the LAT-RM, however the difference is not statistically significant. Also, the coefficient of determination (R^2) shows that 30% of the BSR is explained by the RAR for the proposed method as opposed to 24% for the LAT-RM.

Table 1 Number of reconstructed rib pairs for each thoracic level

Thoracic level	T1	T2	T3	T4	T5	T6	T7	T8	T9	T10	T11	T12
Proposed method	10	10	10	10	10	10	10	10	10	9	9	7
LAT-RM	0	0	0	0	2	6	9	10	10	10	10	10

Point to point distances are also computed using the procedure described in 3.1. The mean distance between the proposed method and the LAT-RM method is 5.03 mm (±4.46 mm).

3.3. Comparison with the PA20-RM

To determine if our predicted ribs are of sufficient reliability, they are compared, using the same procedure described in section 3.1, to those obtained from the method proposed in [9] that is routinely used at SJH. This evaluation is done for the brace group and the preoperative group, to demonstrate that our technique is able to predict the upper rib cage in both cases.

For the 10 brace patients, the average distance for all predicted ribs is 12.19 mm (±8.41 mm). For the 5 preoperative patients, the average distance for all predicted ribs is 11.15 mm (±7.47 mm). For the purpose of visual comparison, Fig. 8 shows the superimposed wireframe reconstructions of the rib cage of a typical patient. It is clear that the proposed method produces much smoother ribs than the PA20-RM, especially in the lateral and axial views.

4. Discussion

A personalized 3D model of the rib cage is essential for clinicians to assess the scoliotic deformities of the whole trunk. A 3D model will not only improve the quality of their evaluation, but it will also help them better understand the complex relationships between the spine, the rib cage and the external trunk surface.

Our results using the gold standard show what Séoud *et al.* already demonstrated, i.e. that a reconstruction using the lateral view gives better results than a reconstruction using the PA-20. This confirms that this latter X-ray view should never be acquired, since it subjects the patient to more radiation with little or no

benefit in return. Also, we can see that for the proposed method, the errors are almost constant over the different scoliotic configurations (Fig. 7), with the average error being slightly higher for the 0° configuration. Contrary to the PA20-RM, for which the errors are nearly twice as high for the non-scoliotic configuration, our method can be used for the reconstruction of the rib cage of non-scoliotic patients. However, the ribs of level T2 show higher errors than the others (Fig. 7a). This can be explained by the fact that these ribs were nearly horizontal in the synthetic model, and the lack of visibility of the most posterior points due to the superposition with the spine generated paraboloids with wrong orientations. Moreover, the ribs that have the highest errors coincide with those whose most posterior points were not detected in the lateral view, i.e. they were detected from the most anterior point to the last visible point just before the spine (due to visibility constraints). This indicates that it is very important to detect a rib from the most posterior point to the most anterior point, as this will ensure that the correct paraboloid is generated.

Séoud *et al.* [13] used a manual selection of 11 points per rib in the PA-0 view, as introduced in [9], and 3 points per rib in the LAT. As in our case, they could not detect the upper half of the rib cage of real patients due to visibility constraints. However, we can nonetheless reconstruct the entire rib cage thanks to our predictive model. Moreover, for the ribs that were detected by both methods, we have shown that using a semi-automatic detection algorithm in the PA-0 and an interactive edge segmentation in the LAT gives a better clinical assessment, as we get a better correlation between the internal and external rib humps. Even if we did not have a statistically significant difference due to our limited sample size, we believe that with more samples we could obtain a significant difference. Thus, our method can be used for the clinical assessment of rib cage deformities.

When comparing the predicted ribs for the brace and preoperative cohorts against their reconstructions with the PA20-RM, the average distances seem high. But in reality, they are within the precision of the PA20-RM found using the gold standard. The maximum average distance is 15.58 mm for the brace cohort and 13.95 mm for the preoperative cohort. These values lie within the precision range of 14.05 mm

(±9.59 mm) found for the 40° scoliotic configuration with the PA20-RM. This indicates that even if our predicted ribs are only approximations, they have the same level of quality as the ribs produced by the PA20-RM.

However, our results also indicate that the predicted ribs can present certain degeneracies or protrusions, for both the brace and preoperative patients. The reason is that the scaling function is not entirely related to the real scale differences between rib levels. Since we use the area of the detected ribs in the PA-0 view to compute our scaling ratios, we lose the depth component of the scaling. Furthermore, the ratios are dependent upon the extent of rib detection, meaning that if a rib was not detected to its full extent, it will have a smaller computed area than one that has been fully detected. Thus, with a scaling ratio larger (or smaller) than the real value, the optimization of the projection error in the PA-0 view will not find the correct solution. Therefore, it is clear that better methods to scale the predicted ribs should be investigated.

Also, the use of a database in our predictive model to generate a mean orientation per vertebral level could be questioned because of its limited number of samples and its limited variability. Furthermore, this database was generated using data coming from the PA20-RM method, which could limit its accuracy.

The technique used at SJH for the 3D reconstruction of the rib cage requires about two hours to complete, since it relies on the manual selection of 11 points per rib in two radiographic views (PA-0 and PA-20), hence a total of 22 points per rib. Our method makes use of a semi-automatic detection of the ribs [16] in the PA-0 view and an interactive selection of a sufficient number of points in the LAT, which is about three time faster. This is an important factor favoring the new method over the current one for the clinical setting.

5. Conclusion

In this article, we have proposed a novel technique for the 3D reconstruction of the rib cage, based on two standard radiographs commonly acquired in orthopedic clinics. We have demonstrated that using the LAT

view, as opposed to the PA20-RM, greatly enhances the reconstruction accuracy and allows the reconstruction and evaluation of non-scoliotic patients' rib cages. Compared to the LAT-RM, we have proved that using a semi-automatic detection of the ribs in the frontal plane and an interactive identification of the rib contours in the lateral view gives better results in terms of clinical assessment. Further, our method not only improves the reconstruction of the lower half of the rib cage, it can reconstruct the upper half despite the high degree of overlapping structures in the LAT view. Although the predicted portions our rib cage reconstructions present some anomalies, they are of the same quality as the PA20-RM.

Furthermore, a personalized 3D rib cage model could be valuable in the context of numerical simulation. First, it would enhance the simulation of the effect of treatment or of scoliosis progression on the shape of the skeletal trunk, and second, it would allow the simulated spine and rib cage shapes to be propagated to the external trunk surface. The latter becomes possible when the reconstruction of the spine and rib cage produces a complete 3D surface model (or at least a form that enables the attachment of soft tissues), not just a wireframe model. This would benefit orthopedic surgeons in finding the appropriate strategy for spinal correction while ensuring the patient's satisfaction.

In future work, a significant improvement of our approach will be to determine a new way to compute the scaling of the predicted ribs. This will greatly improve the quality of the reconstruction of the upper portion of the rib cage. Furthermore, we would like to analyze the impact of the predictive model and try alternate approaches such as using a similar patient to the one being reconstructed to infer the orientation and size of the ribs.

Acknowledgments

The authors would like to thank Philippe Debanné and Lama Séoud for their valuable help and useful comments. Also, we thank Johan Le Bras and Christian Bellefleur for providing the gold standard data.

Competing interests: None declared

Funding: The authors of this manuscript acknowledge the funding of the Natural Sciences & Engineering Research Council of Canada and of the Canadian Institutes of Health Research. The first author also acknowledges a scholarship from the Fonds de recherche du Québec - Nature et technologies, which partially funded his graduate studies. Furthermore, these funding agencies had no involvement in the carrying out of this study nor in the preparation of this manuscript.

Ethical approval: All subjects in this study were enrolled on a voluntary basis and were recruited from the scoliosis clinic of Sainte-Justine Hospital. The patients and their parents/tutors were informed of the nature of the research project by a research nurse and the participants signed an informed consent form. Our research protocol was equally reviewed and accepted by the Research Ethics Committees of Sainte-Justine Hospital and of École Polytechnique de Montréal.

References

[1] Graf H, Hecquet J, Dubousset J. **3-dimensional approach to spinal deformities. Application to the study of the prognosis of pediatric scoliosis**. *Rev Chir Orthop Reparatrice Appar Mot*. 1983;69:407-16.

[2] Villemure I, Aubin CE, Grimard G, Dansereau J, Labelle H. **Evolution of 3D Deformities in Adolescents with Progressive Idiopathic Scoliosis**. *Studies in health technology and informatics*. 2002;91:54-8.

[3] Delorme S, Labelle H, Aubin C-E, de Guise JA, Rivard CH, Poitras B, et al. **Intraoperative Comparison of Two Instrumentation Techniques for the Correction of Adolescent Idiopathic Scoliosis: Rod Rotation and Translation**. *Spine*. 1999;24:2011.

[4] Delorme S, Labelle H, Poitras B, Rivard C-H, Coillard C, Dansereau J. **Pre-, Intra-, and Postoperative Three-Dimensional Evaluation of Adolescent Idiopathic Scoliosis**. *Journal of Spinal Disorders and Techniques*. 2000;13:93-101.

[5] Duong L, Mac-Thiong J-M, Cheriet F, Labelle H. **Three-dimensional Subclassification of Lenke Type 1 Scoliotic Curves**. *Journal of Spinal Disorders and Techniques*. 2009;22:135-43.

[6] Papin P, Labelle H, Delorme S, Aubin CE, de Guise JA, Dansereau J. **Long-term three-dimensional changes of the spine after posterior spinal instrumentation and fusion in adolescent idiopathic scoliosis**. *European Spine Journal*. 1999;8:16-21.

[7] Erkula G, Sponseller PD, Kiter AE. **Rib deformity in scoliosis**. *European Spine Journal*. 2003;12:281-7.

[8] Goldberg CJ, Moore DP, Fogarty EE, Dowling FE. **Surface Topography and the Several Components of Scoliotic Deformity**. *Studies in health technology and informatics*. 2002;88:67-9.

[9] Dansereau J, Stokes IAF. **Measurements of the three-dimensional shape of the rib cage**. *Journal of Biomechanics*. 1988;21:893-901.

[10] Marcil E. **Incorporation du déplacement du patient dans la reconstruction radiographique 3-D de la cage thoracique et du rachis humain**. Master's thesis. Montréal, Canada: École Polytechnique de Montréal; 1996.

[11] Benameur S, Mignotte M, Destrempes F, De Guise JA. **Three-dimensional biplanar reconstruction of scoliotic rib cage using the estimation of a mixture of probabilistic prior models**. *IEEE Transactions on Biomedical Engineering*. 2005;52:1713-28.

[12] Jolivet E, Sandoz B, Laporte S, Mitton D, Skalli W. **Fast 3D reconstruction of the rib cage from biplanar radiographs**. *Medical and Biological Engineering and Computing*. 2010;48:821-8.

[13] Seoud L, Cheriet F, Labelle H, Dansereau J. **A Novel Method for the 3-D Reconstruction of Scoliotic Ribs From Frontal and Lateral Radiographs**. *IEEE Transactions on Biomedical Engineering*. 2011;58:1135-46.

[14] Dworzak J, Lamecker H, von Berg J, Klinder T, Lorenz C, Kainmüller D, et al. **3D reconstruction of the human rib cage from 2D projection images using a statistical shape model**. *International Journal of Computer Assisted Radiology and Surgery*. 2010;5:111-24.

[15] Koehler C, Wischgoll T. **Knowledge-Assisted Reconstruction of the Human Rib Cage and Lungs**. *IEEE Computer Graphics and Applications*. 2010;30:17-29.

[16] Plourde F, Cheriet F, Dansereau J. **Semiautomatic Detection of Scoliotic Rib Borders From Posteroanterior Chest Radiographs**. *IEEE Transactions on Biomedical Engineering*. 2012;59:909-19.

[17] Deschenes S, Charron G, Beaudoin G, Labelle H, Dubois J, Miron M, et al. **Diagnostic imaging of spinal deformities: reducing patients radiation dose with a new slot-scanning X-ray imager**. *Spine*. 2010;35:989-94.

[18] Bellefleur C, Dansereau J, Koller A, Labelle H. **Evaluation of the efficiency of patient stabilization devices for 3D X-ray reconstruction of the spine and rib cage**. *Studies in health technology and informatics*. 2002;88:127-31.

[19] Cheriet F, Laporte C, Kadoury S, Labelle H, Dansereau J. **A Novel System for the 3-D Reconstruction of the Human Spine and Rib Cage From Biplanar X-Ray Images**. *IEEE Transactions on Biomedical Engineering*. 2007;54:1356-8.

[20] Pazos V, Cheriet F, Danserau J, Ronsky J, Zernicke R, Labelle H. **Reliability of trunk shape measurements based on 3-D surface reconstructions**. *European Spine Journal*. 2007;16:1882-91.

[21] Kadoury S, Cheriet F, Laporte C, Labelle H. **A versatile 3D reconstruction system of the spine and pelvis for clinical assessment of spinal deformities**. *Medical and Biological Engineering and Computing*. 2007;45:591-602.

[22] Delorme S, Petit Y, de Guise JA, Labelle H, Aubin CE, Dansereau J. **Assessment of the 3-D reconstruction and high-resolution geometrical modeling of the human skeletal trunk from 2-D radiographic images**. *IEEE Transactions on Biomedical Engineering*. 2003;50:989-98.

[23] Vallieres E. **The Costovertebral Angle**. *Thoracic Surgery Clinics*. 2007;17:503-10.

[24] Graeber GM, Nazim M. **The Anatomy of the Ribs and the Sternum and Their Relationship to Chest Wall Structure and Function**. *Thoracic Surgery Clinics*. 2007;17:473-89.

[25] Poulin F. **Reconstruction et modélisation du col costal à l'aide de radiographies numériques**. Master's thesis. Montréal, Canada: École Polytechnique de Montréal; 1996.

[26] Solution Technologies Inc. **MicroScribe 3D Digitizers**; 2011. http://www.3d-microscribe.com/index.htm [online].

Fig. 1. Extraction of the head and the tubercle from a typical rib. Adapted from [25].

Fig. 2. Rib segmentation in the PA-0 (a) and LAT (b) views.

Fig. 3. Mean and standard deviation of the rib plane orientations per thoracic level.

Fig. 4. Definition of a rib area.

Fig. 5. Generation of the contour surface.

Fig. 6. Reconstruction of a typical rib cage. (a) The ribs' surfaces. (b) The external (red) and internal (green) contours used to generate the surface of a rib. (c) The projection of the external and internal contours on the PA-0 view.

Fig. 7. Evaluation of the distance between the gold standard and the proposed method, and between the gold standard and the PA20-RM for the 0°, 20° and 40° configurations (top, middle and bottom).

Fig. 8. Comparison of the reconstructed ribs with the proposed method (blue) and the PA20-RM (red), for a typical patient, in the frontal view (a), lateral view (b) and axial view (c).

Fig 1

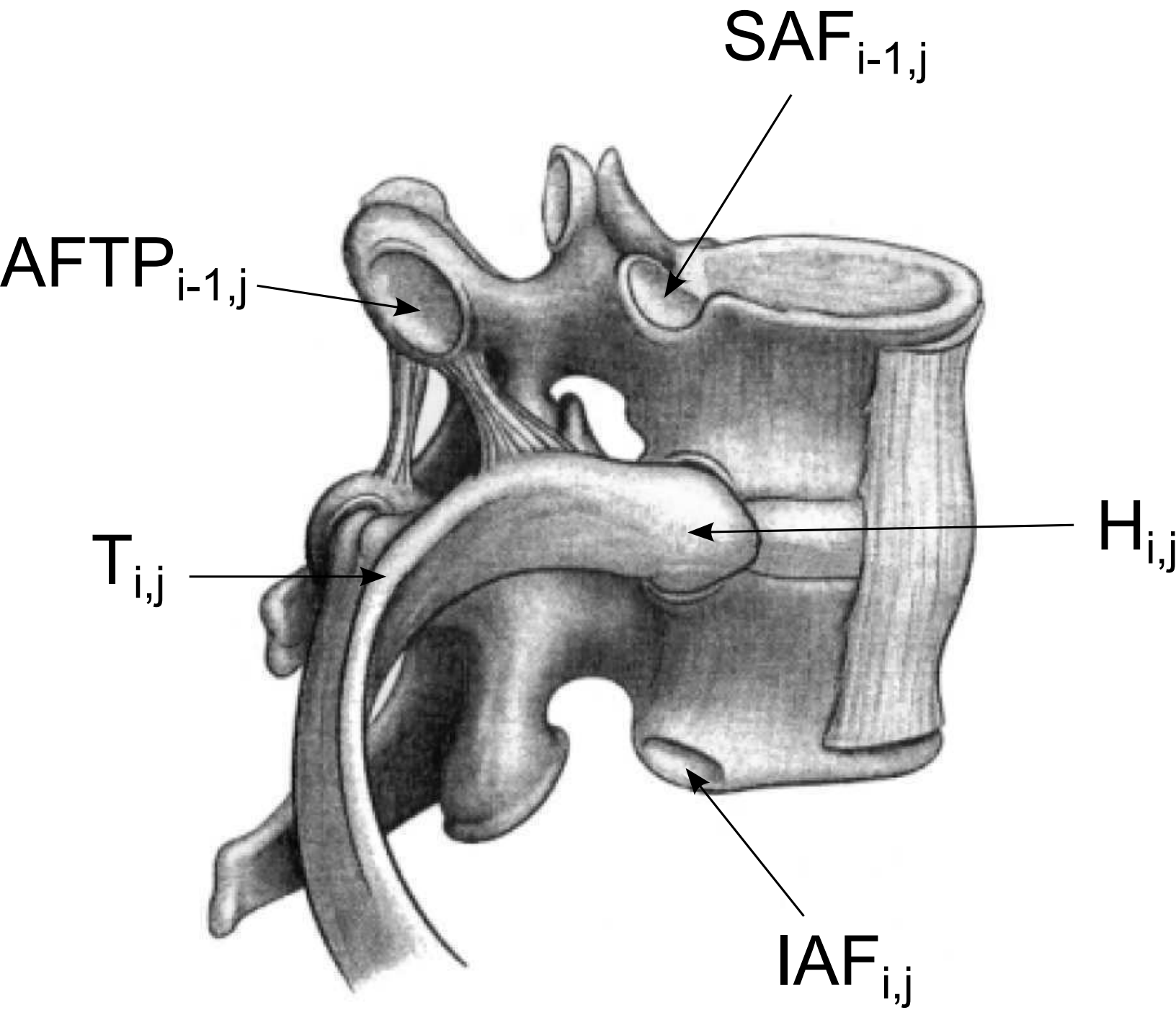

Fig 2

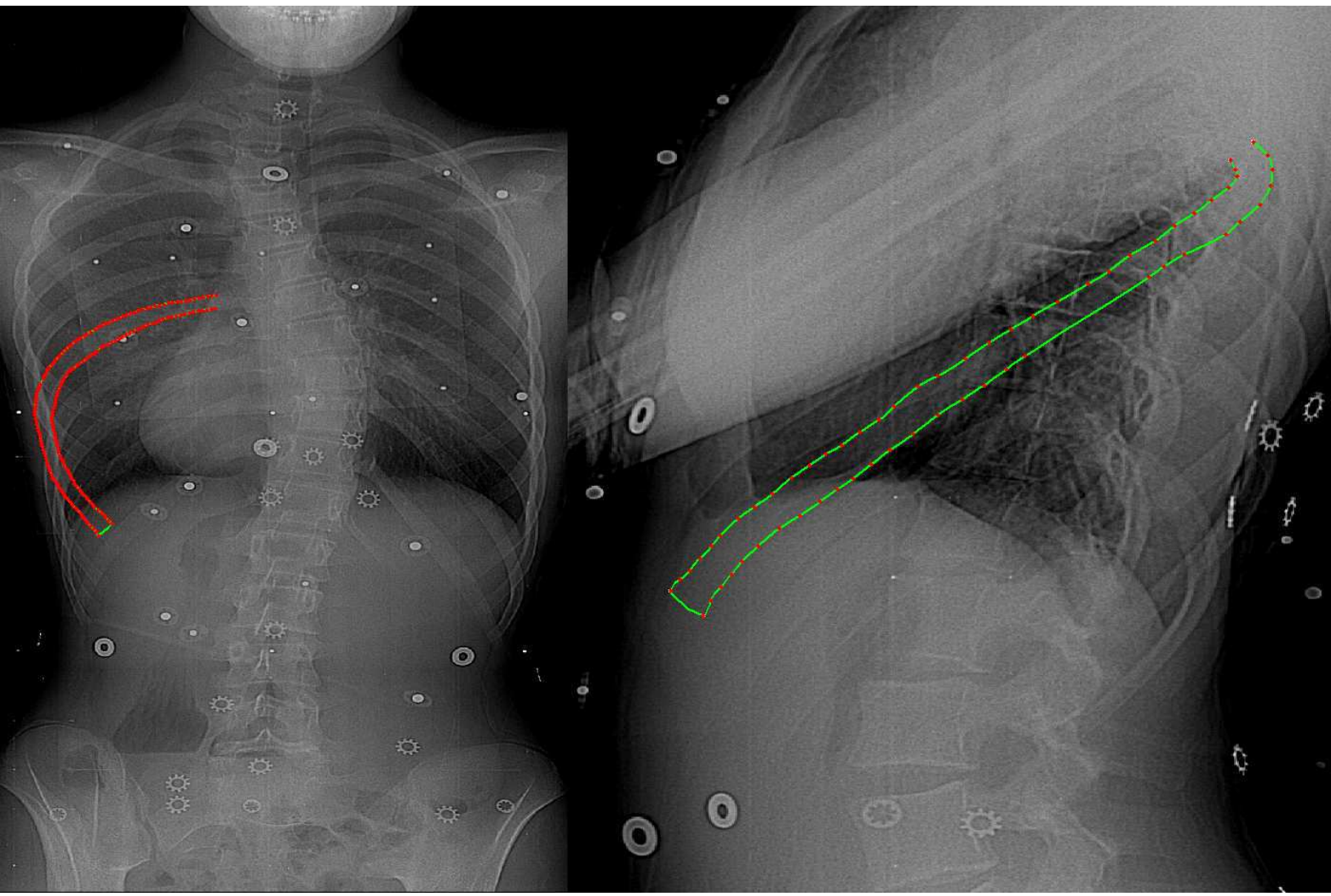

(a) (b)

Fig 3

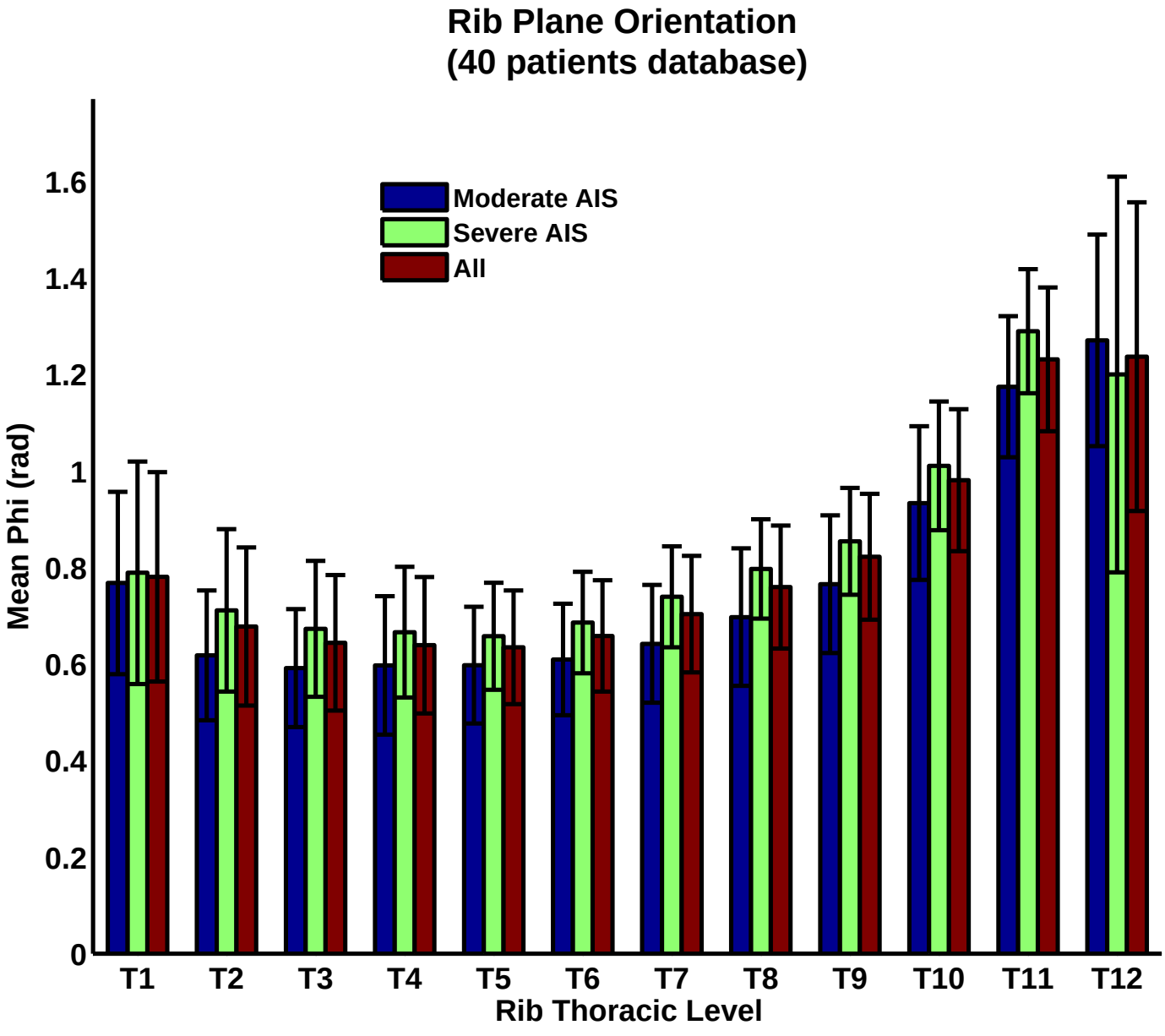
Rib Plane Orientation
(40 patients database)
Moderate AIS
Severe AIS
All
Mean Phi (rad)
0
0.2
0.4
0.6
0.8
1
1.2
1.4
1.6
T1
T2
T3
T4
T5
T6
T7
T8
T9
T10
T11
T12
Rib Thoracic Level

Fig 4

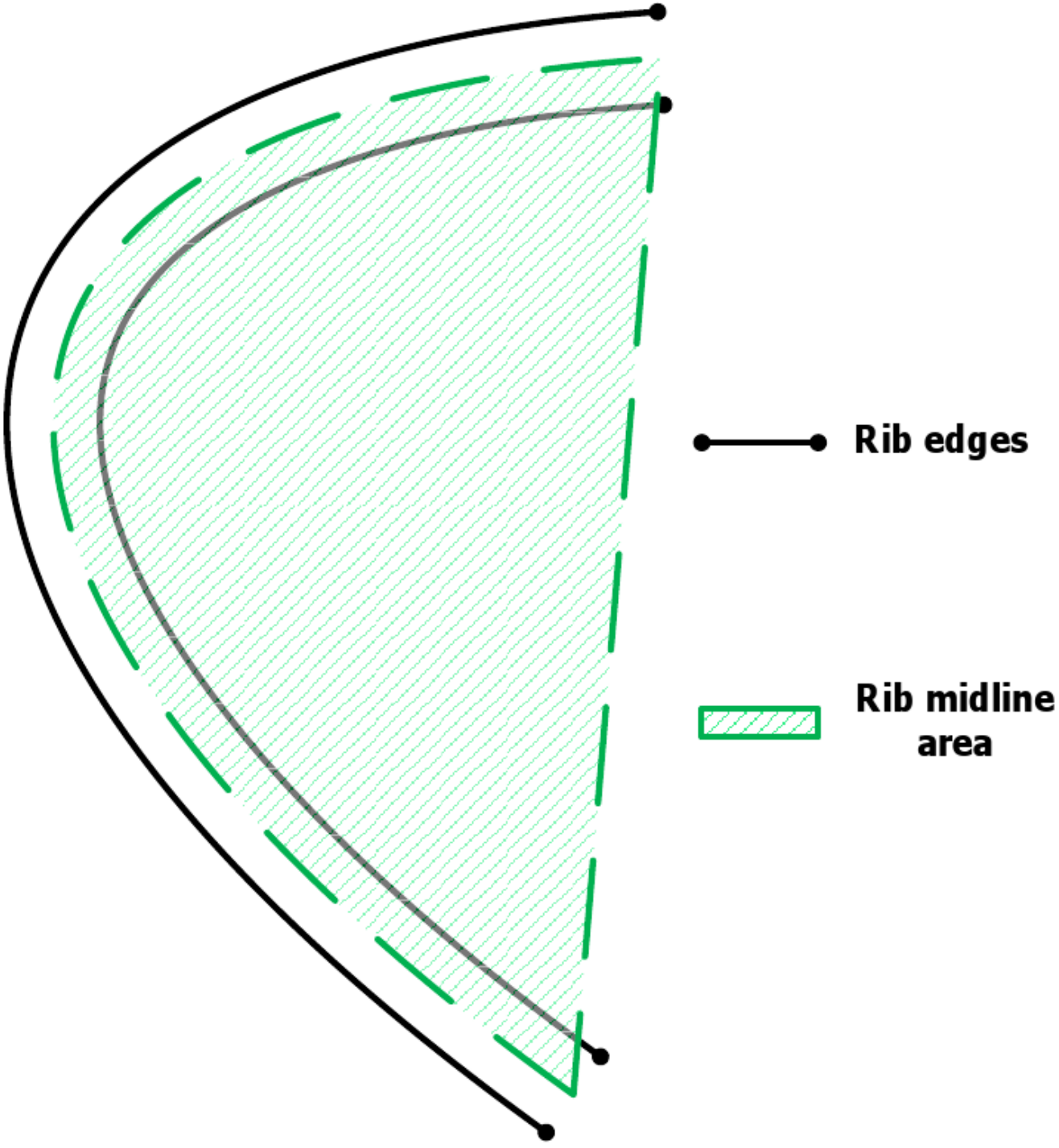

Fig 5

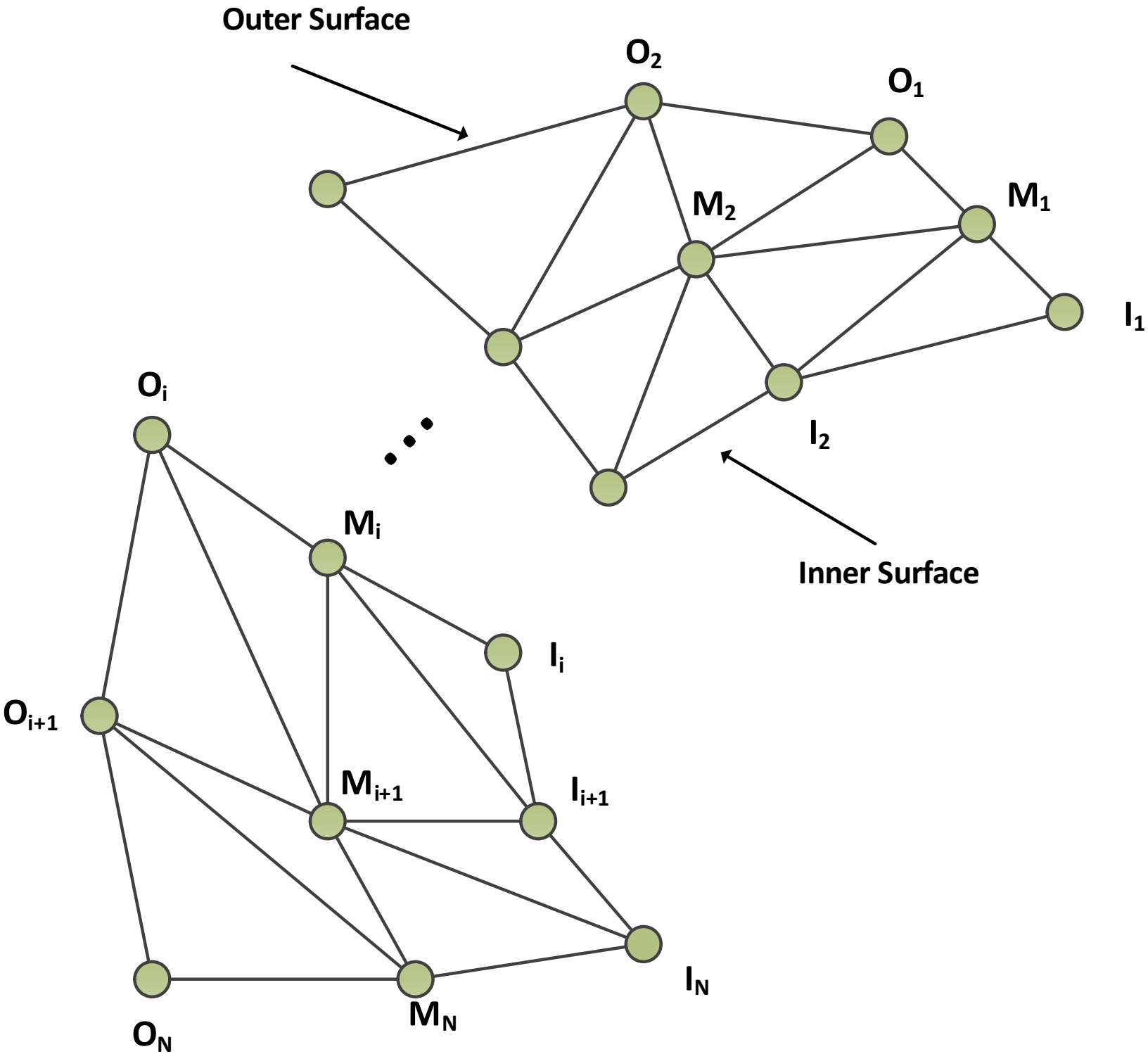
Outer Surface
O2
O1
M2
M1
I1
I2
Oi
Mi
Ii
Oi+1
Mi+1
Ii+1
IN
MN
ON
Inner Surface

Fig 6

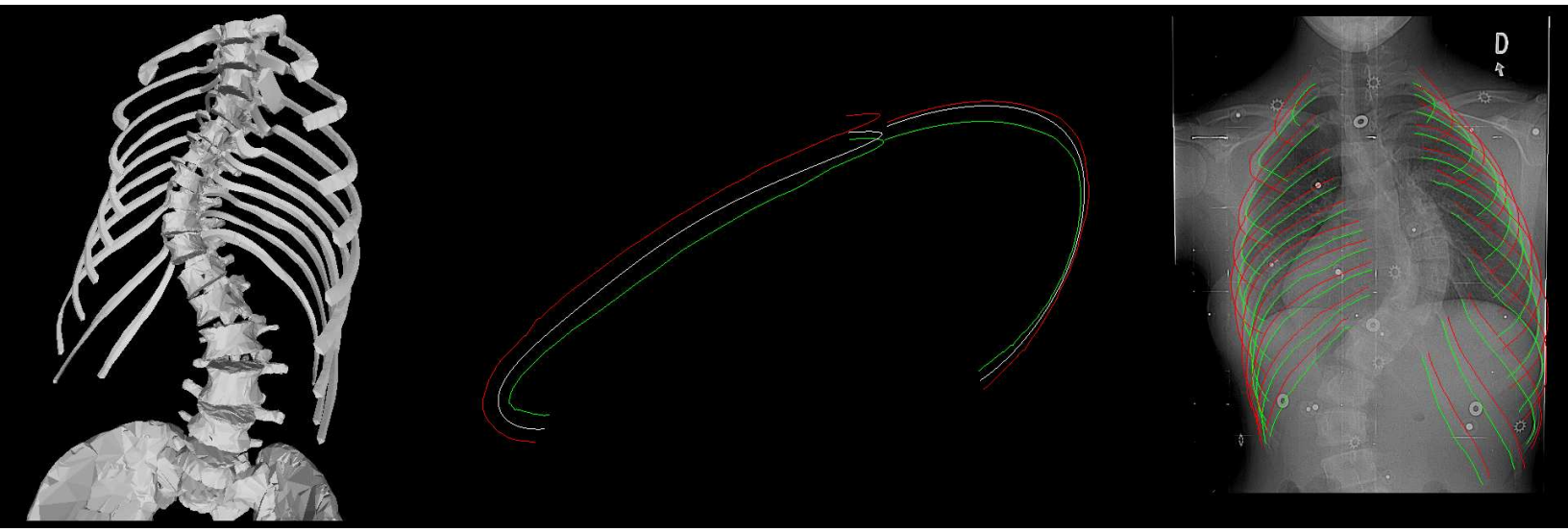

(a) (b) (c)

Fig 7

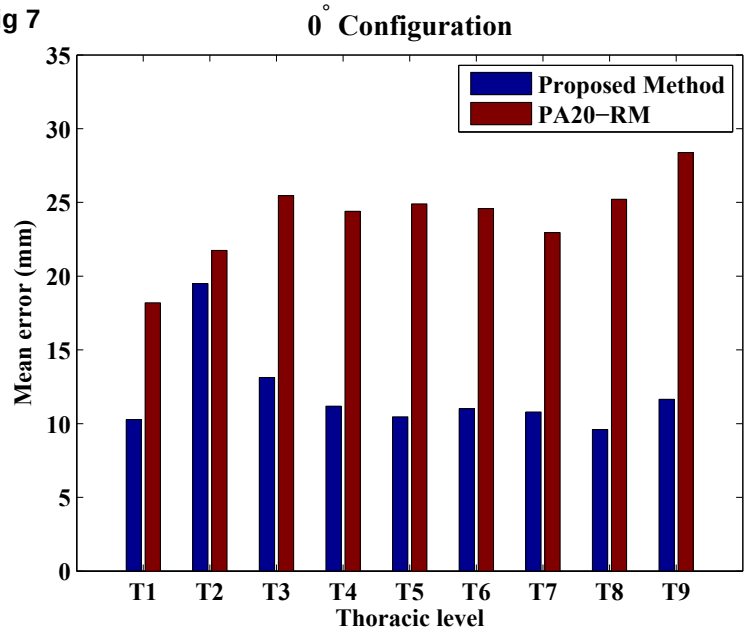
0° Configuration
Proposed Method
PA20−RM
Mean error (mm)
0
5
10
15
20
25
30
35
T1
T2
T3
T4
T5
T6
T7
T8
T9
Thoracic level

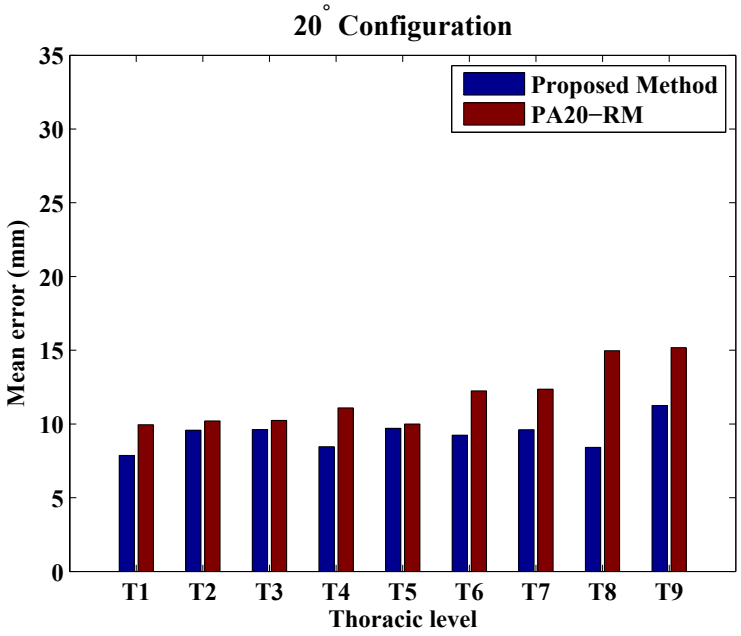
20° Configuration
Proposed Method
PA20−RM
Mean error (mm)
0
5
10
15
20
25
30
35
T1
T2
T3
T4
T5
T6
T7
T8
T9
Thoracic level

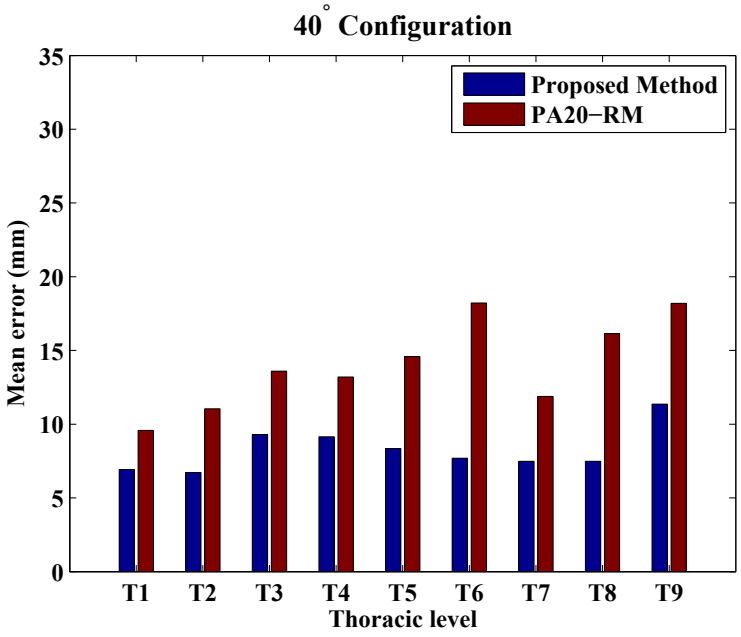
40° Configuration
Proposed Method
PA20−RM
Mean error (mm)
0
5
10
15
20
25
30
35
T1
T2
T3
T4
T5
T6
T7
T8
T9
Thoracic level

Fig 8